CARBON 69 (2014) 178–187

Available at www.sciencedirect.com

ScienceDirect

journal homepage: www.elsevier.com/locate/carbon

Reversible tailoring of mechanical properties of carbon nanotube forests by immersing in solvents

Parisa Pour Shahid Saeed Abadi [a], Matthew R. Maschmann [b,c], S.M. Mortuza [d], Soumik Banerjee [d], Jeffery W. Baur [b], Samuel Graham [a,e], Baratunde A. Cola [a,e,*]

[a] George W. Woodruff School of Mechanical Engineering, Georgia Institute of Technology, 771 Ferst Drive, Atlanta, GA 30332, USA
[b] Air Force Research Laboratory, Materials and Manufacturing Directorate, AFRL/RX, Wright-Patterson Air Force Base, OH 45433, USA
[c] Universal Technology Corporation, Beavercreek, OH 45432, USA
[d] School of Mechanical and Materials Engineering, Washington State University, Pullman, WA 99164, USA
[e] School of Materials Science and Engineering, Georgia Institute of Technology, 771 Ferst Drive, Atlanta, GA 30332, USA

ARTICLE INFO

Article history:
Received 15 July 2013
Accepted 2 December 2013
Available online 7 December 2013

ABSTRACT

The mechanical behavior of carbon nanotube (CNT) forests soaked in three solvents – toluene, acetonitrile, and isopropanol – is examined. Effective stiffness of the structure is evaluated in the dry and wet condition by micro-indentation using a 100 μm flat punch. With soaking of CNT forests in solvents, the stiffness decreases and deformation mechanism changes from buckling concentrated close to the bottom of the CNT forest to a distribution of local buckles along the height and global buckling of the entire length of CNTs. We use molecular dynamics simulations to relate the experimental observations to the reduced mechanical support from neighbor CNTs due to a decreased magnitude of van der Waals (vdW) interactions in the presence of solvents. Toluene, which produces the lowest average measured stiffness between the three solvents, produces the lowest vdW forces between individual CNTs. Furthermore, wet–dry cycling of CNT forests shows the reversibility and repeatability of change of stiffness by immersing in solvents. The results show that soaking CNT forests in solvents could be useful for applications such as interface materials where lower stiffness of CNT forests are needed and applications such as energy absorbing materials in which re-setting of stiffness is required.

1. Introduction

Mechanical behavior of CNT forests has been investigated [1–22] for fundamental understanding of the behavior of these complex nanostructures and to find ways to alter their properties for different applications. CNT forests have been shown to deform under compression primarily with the formation of local buckles along their heights. During flat punch indentations, in addition to local buckles, vertical shear offsets form under the indenter edges at sufficiently high loads [14]. The morphological characteristics of CNTs such as density, orientation, and entanglement have been shown to impact the mechanical properties [1–4,14–16] and deformation mechanism [7,9,14]. For instance, different density and tortuosity profiles along the height of CNT forests have been shown to dictate the location of incipient buckling in CNT forests [14]. All these studies suggest that the interaction between individual CNTs, which is through van der Waals (vdW) forces, affects the collective

* Corresponding author.
E-mail address: cola@gatech.edu (B.A. Cola).
0008-6223/$ - see front matter © 2013 Elsevier Ltd. All rights reserved.
http://dx.doi.org/10.1016/j.carbon.2013.12.004

Report Documentation Page

Form Approved
OMB No. 0704-0188

1. REPORT DATE	2. REPORT TYPE	3. DATES COVERED
2014		**00-00-2014 to 00-00-2014**

4. TITLE AND SUBTITLE	5a. CONTRACT NUMBER
Reversible tailoring of mechanical properties of carbon nanotube forests by immersing in solvents	5b. GRANT NUMBER
	5c. PROGRAM ELEMENT NUMBER
6. AUTHOR(S)	5d. PROJECT NUMBER
	5e. TASK NUMBER
	5f. WORK UNIT NUMBER
7. PERFORMING ORGANIZATION NAME(S) AND ADDRESS(ES) **Georgia Institute of Technology,George W. Woodruff School of Mechanical Engineering,771 Ferst Drive,Atlanta,GA,30332**	8. PERFORMING ORGANIZATION REPORT NUMBER
9. SPONSORING/MONITORING AGENCY NAME(S) AND ADDRESS(ES)	10. SPONSOR/MONITOR'S ACRONYM(S)
	11. SPONSOR/MONITOR'S REPORT NUMBER(S)

12. DISTRIBUTION/AVAILABILITY STATEMENT
Approved for public release; distribution unlimited

13. SUPPLEMENTARY NOTES

14. ABSTRACT

The mechanical behavior of carbon nanotube (CNT) forests soaked in three solvents ? toluene acetonitrile, and isopropanol ? is examined. Effective stiffness of the structure is evaluated in the dry and wet condition by micro-indentation using a 100 lm flat punch. With soaking of CNT forests in solvents, the stiffness decreases and deformation mechanism changes from buckling concentrated close to the bottom of the CNT forest to a distribution of local buckles along the height and global buckling of the entire length of CNTs. We use molecular dynamics simulations to relate the experimental observations to the reduced mechanical support from neighbor CNTs due to a decreased magnitude of van derWaals (vdW) interactions in the presence of solvents. Toluene, which produces the lowest average measured stiffness between the three solvents, produces the lowest vdW forces between individual CNTs. Furthermore, wet?dry cycling of CNT forests shows the reversibility and repeatability of change of stiffness by immersing in solvents. The results show that soaking CNT forests in solvents could be useful for applications such as interface materials where lower stiffness of CNT forests are needed and applications such as energy absorbing materials in which re-setting of stiffness is required.

15. SUBJECT TERMS

16. SECURITY CLASSIFICATION OF:			17. LIMITATION OF ABSTRACT	18. NUMBER OF PAGES	19a. NAME OF RESPONSIBLE PERSON
a. REPORT	b. ABSTRACT	c. THIS PAGE			
unclassified	**unclassified**	**unclassified**	**Same as Report (SAR)**	**10**	

mechanical response of CNT forests. The extent of this influence requires further investigation and is the focus of this work.

VdW forces are intermolecular bonding forces due to interaction between permanent or induced dipoles and change by altering the medium through which the objects interact [23]. We use this fact to intentionally manipulate the interaction between CNTs in forests. We examine the mechanical behavior of the CNT forests in the presence of solvents in an effort to investigate the effect of interaction between individual CNTs on the collective mechanical behavior of CNT forests. The effects of capillary forces, due to evaporation of fluids such as solvents, on densification and self-assembly of CNT forests have been investigated [24–31] and significant increases in the elastic modulus of the CNT forests because of the densification have been measured [28,29]. However, the mechanical properties of the CNT forests in the presence of solvents have not been investigated. In addition to fundamental understanding of the factors affecting the mechanical response of CNT forests, this knowledge is necessary for the analysis of self-assembly due to capillary forces and also for applications where a CNT forest wetted by a solvent is under mechanical loading [32,33]. In the latter case, solvent wetting was used in a process to coat CNT forest thermal interface materials at their tips with organic bonding agents to improve thermal conductance at the contact surface.

Here, we investigate the compressive response and deformation mechanism of CNT forests in the presence of solvents by flat punch micro-indentation. We report reduction in stiffness relative to the as-grown state after CNT forests are immersed in solvents. We also report increase in stiffness relative to the immersed state when the CNT forests are densified after solvent evaporation. Further, we find that the stiffness changes between the softened solvent-immersed state and densified state are reversible and repeatable. Post-evaporation scanning electron microscopy (SEM) imaging of CNT forests that were compressed in the presence of solvents and dried under compression reveals that the deformation mechanism changes from local buckling close to the substrate to the formation of local buckles distributed along the height and global buckling of CNTs. Three solvents – toluene, acetonitrile, and IPA – are used to further investigate the relation between vdW forces and stiffness of the CNT forests. Toluene is shown to produce larger reductions in stiffness than IPA and acetonitrile. The effect of the three solvents on the vdW forces between individual CNTs are quantified using molecular dynamics (MD) simulations. The vdW forces between individual CNTs in toluene are found to be lower than in the other two solvents. Our results quantify the effect of vdW forces between CNTs on the stiffness of CNT forests. They also show how the change in interaction between CNTs affects the buckling behavior. These results demonstrate the importance of interaction between CNTs in the collective mechanical response of CNT forests and could lead to new applications of CNT forests.

2. Experimental

The multiwall CNT forests were grown using a low pressure CVD method on Si substrates coated with Ni (100 nm)/Ti (30 nm)/Al (10 nm)/Fe (3 nm) as the catalyst stack. The growth was performed in an Aixtron Black Magic CVD system at a temperature of 750 °C and a pressure of 10 mbar. Two growth times were used: 10 and 30 min that resulted in height ranges of 25–40 and 115–150 μm, respectively. Acetylene and hydrogen were used with the rates of 100 and 700 sccm respectively. The average diameter and the average number of walls were measured using transmission electron microscopy (TEM) to be 7 nm and 6 respectively. More information on the growth parameters and TEM images are provided in previous work [14].

Micro-indentation testing was performed using a 100 μm diameter cylindrical flat punch in a MTS Nanoindenter XP nanoindentation system. Short (25–40 μm) and long (115–150 μm) CNTs were indented to 10 and 20 μm depth respectively. Strain rate of 0.1 s^{-1} was used except for test where the effect of strain rate was investigated (0.01, 0.1, and 1 s^{-1} were used in this case). First, micro-indentation testing was performed on as-grown samples in air. Then, samples were immersed in a pool of solvent, covering CNT tips, and similar indentation testing was performed on the samples in this state (Fig. 1). The weight of the Si substrates (600 μm thick) prevented the samples from floating in the solvents. Experiments on each sample were performed in a relatively short time before a significant amount of solvent could evaporate and decrease the fluid level. Due to the open top of the pool, the solvent was not constrained and no significant change in load was detected by contact with the solvent surface. This allowed clear detection of the CNT surface immersed in the solvent.

3. Simulation model

Molecular dynamics simulations were performed using Gromacs 4.5.5 MD simulation software [34] and the OPLS-AA (optimized potentials for liquid simulations-all atom) model was employed as the atomistic force field. CNTs with 7 walls, and outermost and innermost diameters of 6.34 and 2.11 nm, respectively, were simulated. These are approximately the same as the average values measured by TEM for the type of CNTs in the forest studied here [14]. The length of each

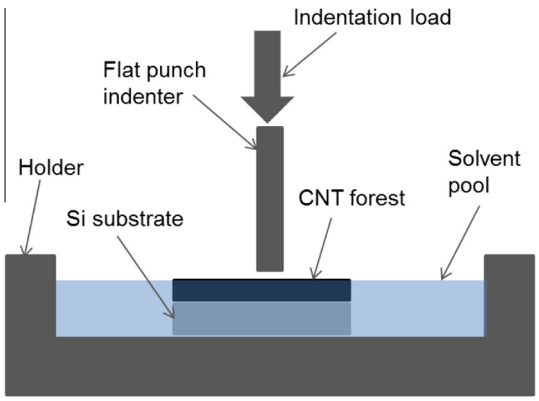

Fig. 1 – Schematic of indentation of a CNT forest inside a solvent pool. (A colour version of this figure can be viewed online.)

simulated CNT was 7 nm. An equilibration run (at least 30 ps) was performed until the total energy of each system reached a minimal value. Following equilibration, a production run was performed for at least 30 ps on a microcanonical ensemble, where number of particles, volume and energy of the system are held constant, to obtain reliable and statistically relevant results. The equations of motion were integrated with a time step of 1 fs. The cutoff distances for vdW interactions were 2.0 nm. In order to quantify the strength of vdW interactions between CNTs, Hamaker constant of CNTs in vacuum, $A_v = V * \frac{12\pi D^2}{G}$, was evaluated where 'V' is the vdW dispersion interaction energy between CNTs, 'D' is the separation distance between two CNTs and 'G' is the effective area for vdW interactions between the CNTs. The vdW dispersion interaction energy V between CNTs was evaluated by summing up the pairwise attractive interactions between atoms of distinct CNTs. The value of 'G' can be defined as $(l \times w)$ and $(w \times w)$ for parallel and perpendicular CNTs respectively, where 'l' is the length and 'w' is the width of interaction of each CNT. The value of 'w' was obtained using the relationship, $w = 2\sqrt{R^2 - \left(R - \frac{D_c - D}{d}\right)^2}$, where 'R' is the radius of the CNT and 'D_c' is the cutoff distance for vdW interactions of CNTs, which is 2.0 nm. Fig. 2 shows the top view of two parallel CNTs where w, R, D_c and D are depicted. As the diameter of the CNT is relatively large (6.34 nm) compared to the cutoff distance for vdW interactions of CNTs (2.0 nm), the atoms of the CNTs that are far removed effectively do not interact with each other. Therefore, we assumed curved surface–surface vdW interaction between two CNTs to evaluate the Hamaker constant.

4. Results and discussion

Mechanical response of the samples was tested by a flat punch in two different mediums: (1) air and (2) immersed in toluene. Each sample was indented on 20 spots to examine the uniformity of the samples. Indentation stress was calculated by dividing the load by the indenter cross section area and indentation strain was calculated by dividing the indenter displacement by the average height of the CNT forest.

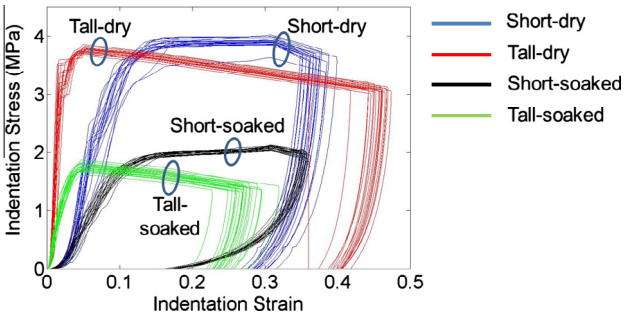

Fig. 3 – Stress–strain curves for dry and toluene-infiltrated CNT forests with initial average height of 30 (short) and 130 μm (tall). (A colour version of this figure can be viewed online.)

The stress–strain curves for the case of in-air (dry) and in-toluene (soaked) testing of short (25–40 μm) and tall (115–150 μm) CNT forests are shown in Fig. 3. The tight distribution of the curves shows the uniformity of the samples. Each stress–strain curve consists of a stiff section up to the strain of ~0.04 and 0.15 for tall and short CNT forests, respectively, followed by a plateau, which continues to the point of unloading. The unloading point started at indentation depth of ~10 μm (strain of ~0.35) for short CNT forests but varied in the tall CNT forests because of instability caused by the indenter sliding into the forest. This sliding instability is associated with a drop in load. Due to the sudden loss of stiffness, the indenter moves faster than the prescribed displacement rate. The tool decreases the load in an effort to decrease the displacement rate. This variation in the unloading depth did not cause a significant change in the measured unloading stiffness. This is supported by the similar slopes in Fig. 3 for points with different indentation depths.

The deformation mechanism of dry CNT forests grown with LPCVD recipe is reported in our previous work [14] using *in situ* indentation. The deformations are shown in Fig. 4a (adapted from our previous paper [14]). Local buckles form progressively from the bottom of CNT forests – i.e., close to the substrate – from the very beginning of indentation at

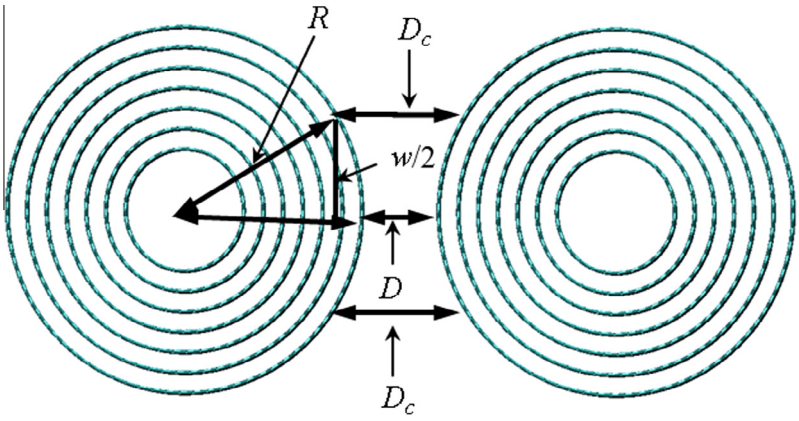

Fig. 2 – Top view of parallel open-ended CNTs. R = radius of the CNT; D_c = cutoff distance for vdW interactions of CNTs; D = separation distance between CNTs; w = width of vdW interactions of CNT. (A colour version of this figure can be viewed online.)

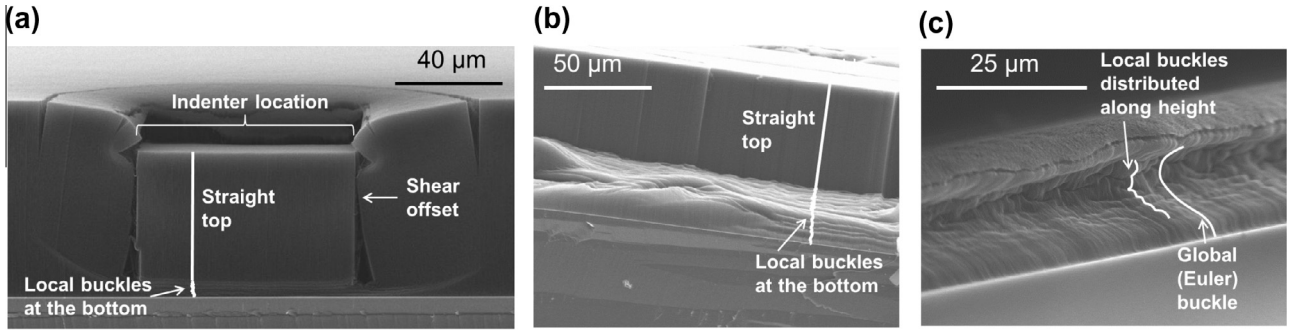

Fig. 4 – Deformation mechanism of dry and wet CNT forests. (a) Dry sample after *in situ* indentation (adapted from Ref. [14] with permission from The Royal Society of Chemistry), (b) dry sample after macro-compression, and (c) wet macrocompressed and then dried.

the initial stiff part of the load–displacement curve. The sudden change of slope and start of the plateau region is related to the formation of shear off-sets (vertical openings under indenter edges that separate CNTs directly under the indenter from the surrounding CNTs) and sliding of the indenter into the CNT forest. Visualization of deformation of the wet samples at the time of indentation is not possible due to the limitations of high magnification SEM imaging in vacuum. Since the plateau regions for dry and wet samples are similar, sliding of the indenter into the CNT forests similar to the case of dry samples likely occurs in wet samples. However, the buckling behavior of the wet forest is still unknown due to a lack of *in situ* observation.

A different method was used to visualize the deformation of wet CNT forests to gain insight into their buckling behavior. We performed macroscale uniaxial compression of dry and wet samples (immersed in toluene) by pressing 1×1 cm samples using known weights to apply pressures up to 700 kPa, which are in the range applied to the samples in the micro-indentation experiments. The range of sample heights was similar to the range of heights tested by micro-indentation, 20–140 μm. All samples were under pressure for more than 6 h to ensure that wet samples were completely dried under pressure. Because of continuous loading in the drying process, the deformation in the wet state is expected to remain within the CNT forest upon drying. Fig. 4b and c shows the side view of two representative deformed CNTs after dry and wet macroscale compression respectively. The buckling of the dry sample (Fig. 4b) is similar to the results of *in situ* indentation of dry CNT forests reported in our previous work [14] and shown in Fig. 4a, i.e., periodic buckling from the bottom of the CNT forest while the top part remained undeformed. Deformation under wet compression is observed to be substantially different from that under dry compression (Fig. 4c). Local buckles were distributed along the height and CNTs were bent globally – i.e., along the entire height – similar to the Euler buckling mode of columns with a fixed bottom end and a supported top end. Lines showing the undeformed parts and local and global buckles are drawn on Fig. 4a–c for clarification. The bent tips after wet compression (Fig. 4c) likely increase the area of CNT to surface contact compared to the case of dry compression with undeformed CNT tips (Fig. 4a,b), which could explain observations of reduced thermal resistance at a solvent soaked interface [32,33].

The major differences between the load–displacement curves for the dry and wet indentation are the stiffness of the CNT forest and the plateau stress. The plateau stress which is related to the formation of shear off-sets decreased from ~4 to ~2 MPa by wetting for both short and long CNT forests. The slope in both initial and unloading sections of the stress–strain curve is smaller for wet samples. Stiffness was measured by the slope of the unloading curve at the beginning of unloading [35]. Wetting the CNT forest with toluene decreased the stiffness from 62.1 ± 13.8 and 36.2 ± 4.0 to 12.1 ± 0.8 and 7.4 ± 0.5 kN/m in the short and long CNT forests, respectively. Harmonic (dynamic) stiffness measurements were also performed with 10 nm amplitude along the indentation path. This method provides unloading stiffness information as a function of indentation depth. The plots showing the trends of harmonic stiffness with indentation depth are shown in Fig. 5. Stiffness increases by increasing depth until the point of shear off-set formation where there is a drop in the stiffness. In both dry and wet states, the maximum harmonic stiffness for the short CNT forest is higher than that for the tall CNT forest. This is consistent with our previous report [14]. The results also show that harmonic stiffness decreases by soaking samples in solvents for both sample heights.

Two other solvents – namely acetonitrile and isopropyl alcohol (IPA) – were used to wet CNT forests and indentation testing was performed on them at a minimum of 10 points. Similar to toluene, these two solvents decreased the stiffness of the CNT forests. The extent of stiffness reduction by solvent infiltration depended on the original stiffness of the CNT forest (i.e., stiffness before hydration). Nine samples with different stiffness were mechanically tested before and after being soaked in the solvents (three samples with each solvent). The reduction in the maximum harmonic stiffness (the stiffness before the formation of shear offsets) versus the original maximum harmonic stiffness is shown in Fig. 6. The error bars show the standard deviation of the values measured at different points on each sample. There is an overall increase in the stiffness reduction with the increase in the initial stiffness of the CNT forests. The relationship ap-

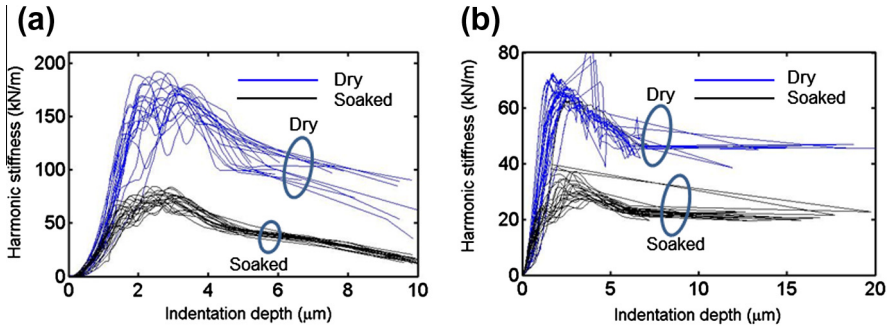

Fig. 5 – Harmonic stiffness for dry and toluene-infiltrated CNT forests with initial average height of (a) 30 μm and (b) 130 μm. (A colour version of this figure can be viewed online.)

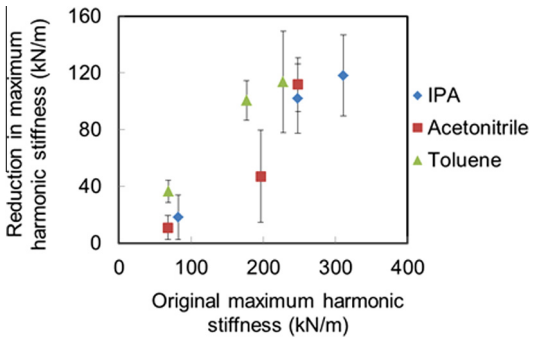

Fig. 6 – Change of reduction in the maximum harmonic stiffness with the original maximum harmonic stiffness for samples wetted with the three solvents. (A colour version of this figure can be viewed online.)

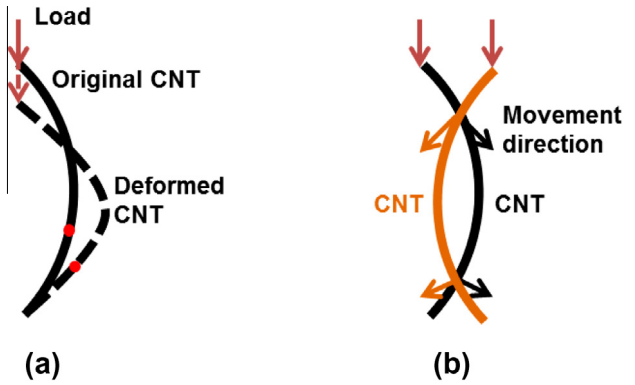

Fig. 7 – (a) Schematic of deformation of a piece of a curved CNT. (b) Schematic of pieces of two CNTs in contact; different preferred directions of movement of CNTs at contact points are shown with arrows. (A colour version of this figure can be viewed online.)

pears to be approximately linear for every solvent with a slope in the range of 0.4–0.5. The difference between the trends for the acetonitrile and IPA is not statistically significant. However, toluene causes slightly larger stiffness reduction compared to the other solvents.

In our previous work [14], we showed that under compressive loading, local CNT aerial density and tortuosity along the height of CNT forests determine the location of incipient buckling within the CNT forests. We suggested that a greater number of contact points between CNTs cause extra constraints, which make the CNTs less prone to bending and buckling. Here we suggest that the effects of solvent on the stiffness and deformation mechanism of the CNT forests are related to the change of constraints at CNT contact points, i.e., the change in strength of the constraint at each existing contact point. We suggest that the collective stiffness of CNT forests can be expressed in a simple form as a combination of two elements,

$$S = S_{ind} + S_{vdW}. \quad (1)$$

The first element (S_{ind}) is the summation of stiffness of individual CNTs such as axial compression stiffness and bending stiffness. This stiffness is equivalent to the stiffness of a CNT forest with similar morphology in which individual CNTs do not "see" each other, i.e., do not interact. The second component (S_{vdW}) originates from the interactions between CNTs – mostly at contact points – which provide mechanical support and constraint opposing deformation. Interaction between CNTs at the contact points is *via* vdW forces which are due to the interaction between induced dipoles [23] of adjacent CNTs. Under compressive loading, a curved piece of a CNT tends to move laterally in addition to the downward deformation. Fig. 7a shows schematically a simple example of this bending behavior and the movement of the red circle demonstrates the lateral movement of the CNT. Because adjacent CNTs can move in three dimensions, there is a high probability that curved CNTs tend to move in different directions at contact points as illustrated in Fig. 7b. The vdW adhesion force between them opposes the deformation in different directions and, therefore, produces a stiffness that is higher than in the case of two non-interacting CNTs. A medium that fills the space between the two CNTs diminishes the dipole–dipole interaction and reduces the vdW force between them. This occurs when any two objects are immersed in a medium [23]. S_{vdW} decreases with the reduction in vdW attraction forces between CNTs and, as a result, the effective stiffness of the CNT forest as measured in the indentation testing (S) decreases. The fact that the reduction in stiffness by solvent increases with the increase in original stiffness (Fig. 6) shows that S_{vdW} is larger for the CNT forests with larger S and, therefore, reduction of the vdW forces has a more significant effect on their stiffness. Larger S_{vdW} in stiffer CNT forests is reasonable to expect because the higher

stiffness is due to an increased density of CNTs in the forest, which would produce a relative increase in S_{vdW}, and/or a reduction in CNT height, which would produce an increased average aerial density of CNTs in the forest [14,36], and consequently a relative increase in S_{vdW}. The effect of solvent on the interaction between CNTs could also be used to explain the change in the buckling behavior (Fig. 4). Property gradients, which cause buckles to be concentrated at the bottom of dry CNT forests, are due to change in the aerial density of CNTs and change in the interaction between CNTs. The latter is less significant in a CNT forest immersed in a solvent due to smaller vdW forces between CNTs. This is likely the reason for the observation of local buckles distributed along the height (not concentrated at the bottom) and also global (Euler) buckling of CNTs in the case of CNT forests in solvent. Euler buckling was previously observed for CNT forests with a lesser degree of tortuosity and interaction [11,14].

While modeling the entire structure of a CNT forest with many high aspect ratio CNTs is difficult and out of scope of this paper, we employed theoretical and numerical tools to quantify the reduction in the vdW forces at individual CNT contact points. This is useful for identifying the distance range in which vdW interactions between individual CNTs are significant and for comparing the effect of different solvents. The values of the vdW forces are directly proportional to Hamaker constant, which depends on the macroscopic properties of the interacting objects and the medium such as dielectric constant and refractive index [37]. Effective value of the Hamaker constant A_{121} for evaluating the vdW forces between similar bodies (1) in a medium (2) can be estimated [23] using the values of Hamaker constant for the medium A_{22} and for the objects in vacuum A_{11},

$$A_{121} = \left(A_{11}^{1/2} - A_{22}^{1/2}\right)^2 \quad (2)$$

We evaluated the vdW interactions between multiwall CNTs in vacuum using molecular dynamics (MD) simulations. The Hamaker constant (A_{22}) of air is approximately zero [38]. Therefore, the Hamaker constant and interaction energy calculated here in vacuum could be considered as the values in air. Since vdW interaction energy between two CNTs varies with the orientation angle between the axes of the CNTs [39], we simulated two distinct configurations where the two CNTs are parallel and perpendicular to each other. The data from these two extreme configurations is expected to approximately determine the range of interaction energy for CNTs at any contact angle. Fig. 8a,b shows the side views of the simulated configurations. From simulations we obtained time-averaged vdW attractive interaction energy, V, and Hamaker constant, A, between two CNTs at different distances for both configurations (details in Section 3). Fig. 8c shows the absolute value (magnitude) of the calculated time-averaged vdW interaction energy between CNTs in vacuum at various separation distances between 0.35 nm (approximately twice the vdW radius of a carbon atom) and 1 nm for parallel and perpendicular configurations. The magnitude of the vdW interaction between CNTs decreases with increased separation distance following a power function relation for both parallel and perpendicular configurations. The vdW interaction between two CNTs at 1 nm distance is at least an order of magnitude weaker than the interaction between two CNTs in contact i.e., ~0.35 nm distance. This further demonstrates that mechanical constraints due to vdW interaction between CNTs are effective primarily at the contact points as conceptualized in Fig. 7b. The vdW interaction between CNTs is greater when they are parallel to each other because a greater number of CNT atoms are in close proximity compared to the perpendicular configuration, especially at relatively small separation distances.

The Hamaker constant of CNTs in vacuum calculated by MD and the Hamaker constant for the solvents – 54 zJ for toluene [23], 42 zJ for acetonitrile [40], and 36 zJ for IPA [41] – were substituted in Eq. (2) to obtain the Hamaker constant for the CNTs in the solvents. Fig. 8d shows the Hamaker constant of CNTs in vacuum and in the three solvents at various distances for both parallel and perpendicular configurations. The results demonstrate that Hamaker constant of CNTs decreases with the increase of distance for all the cases, which qualitatively agrees with results of Rajter et al. [42]. Similar trends are also observed for parallel and perpendicular CNTs in the three solvents. The results illustrate that the Hamaker constant for CNTs is greater in vacuum than that in solvents due to solvent induced reduction of attraction forces. Solvents as the medium reduced the Hamaker constant to ~20–60% of the original value. This range is independent of the length of CNTs. For parallel CNTs, this is because interactions in both dry and wet cases increase with the same ratio by increasing CNT length. For perpendicular CNTs, an increase in CNT length has no effect on interactions between CNTs because the distance between atoms increases with increased CNT length. While acetonitrile and IPA produced similar values of Hamaker constant, toluene produced slightly lower Hamaker constant compared to the other two solvents. This is probably the reason for the similar effects of acetonitrile and IPA on the measured stiffness and higher reduction in stiffness produced with toluene (Fig. 6). Toluene producing the lowest Hamaker constant and highest stiffness reduction provides evidence of the significant effect of vdW forces on the collective stiffness of the CNT forests.

Wet–dry cycling of CNT forests was performed on multiple samples using different solvents to investigate the repeatability of the tailoring of mechanical properties and further demonstrate the significant effects of altered vdW interactions on mechanical properties. Each cycle included immersing a CNT forest in solvent and then drying at room temperature. Indentation was performed in a minimum of five points on the samples in the wet state and in the dry-out state after solvent evaporation. Wetting and drying for three cycles were performed on a short and a tall CNT forest using acetonitrile. The harmonic stiffness change with indentation depth for the short and long CNT forests are shown in Fig. 9a,b respectively. Furthermore, ten wet–dry cycles were performed on a short CNT forest using IPA to ensure that changing the solvent or increasing the number of cycles does not change the repeatability. The stress–strain and harmonic stiffness curves for this cycling test are shown in Fig. 9c,d respectively. Maximum harmonic stiffness for these three tests on a short CNT forest using acetonitrile, a tall CNT forest using acetonitrile, and a short CNT forest using IPA are shown in Fig. 9e–g respectively. The samples in the wet state have lower stiffness

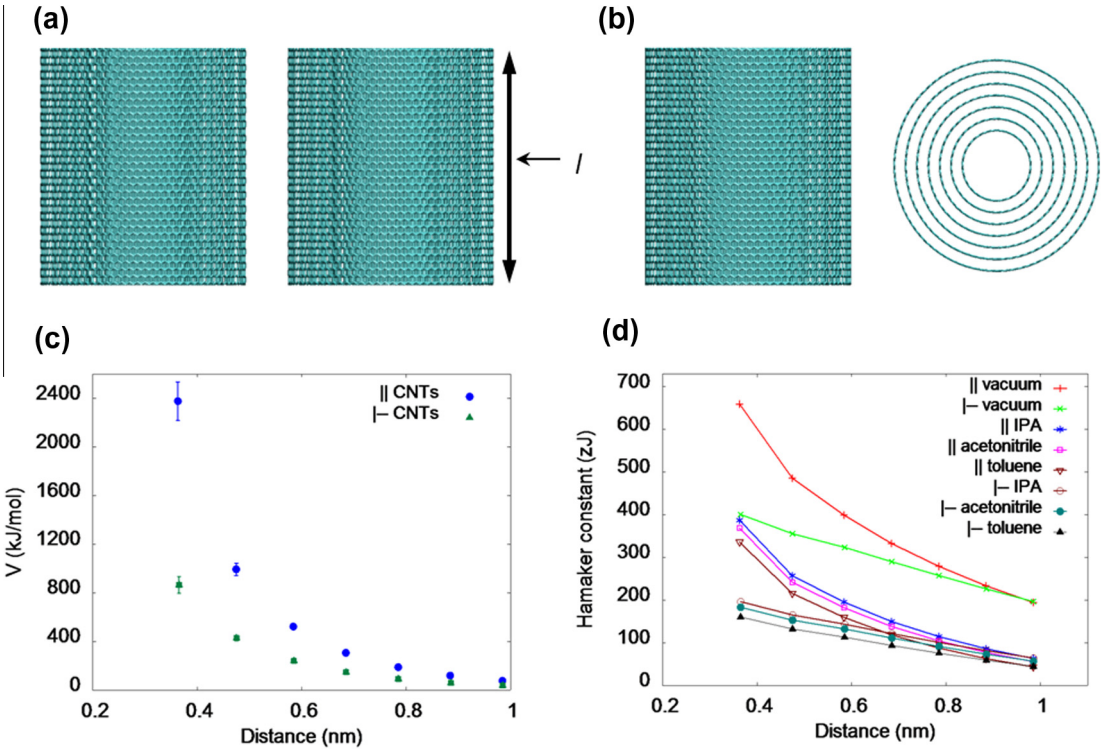

Fig. 8 – Side views of (a) parallel CNTs and (b) perpendicular CNTs. l = length of the CNT. (c) The absolute value of vdW dispersion interaction energy between CNTs in vacuum at various separation distances between them. ||: parallel CNTs; |–: perpendicular CNTs. (d) Hamaker constant of CNTs in vacuum, toluene, acetonitrile, and IPA for both parallel and perpendicular configurations at various separation distances. ||: parallel CNTs and |–: perpendicular CNTs. (A colour version of this figure can be viewed online.)

than the original stiffness, and in the dry-out state they have higher stiffness than in the wet state. All dry-out data points in Fig. 9e–g are enclosed in rectangles for clarification. These trends are independent of the height (in the range tested) and the type of solvent. The higher stiffness at the dry-out state is due to the densification of CNT forests due to capillary forces, which is widely reported [24–31]. The samples at the dry-out state also possess a large variation in the stiffness demonstrated by the error bars, which are on average at least twice as large as the error bars in the original or wet states. This is due to surface non-uniformity after densification; only a part of the indenter area is in contact with the CNT surface, and this contact area varies from point to point. Stiffness in the wet state generally decreases with increased cycles up to the fifth cycle. This is likely due to reconfiguration of the CNT morphology and contacts during evaporation due to capillary forces. The ten cycle test shows that the stiffness at both wet and dry-out states reach a plateau region at the fifth cycle and do not change significantly up to 10 cycles. This shows that the tailoring of mechanical properties of the CNT forest using solvents is repeatable and reversible.

Another scenario to possibly explain the effect of solvent on the stiffness reduction is viscous drag. A fluid flow perpendicular to the CNT nominal alignment direction is produced by the vertical movement of the indenter and applies a transverse load on the CNTs. The CNT forests are expected to be relatively weak in the transverse direction and, therefore, have lower stiffness in this direction. To investigate the significance of this effect or any other load-carrying role of solvents, we performed strain rate testing of CNT forests with and without a solvent. Toluene was chosen and the results are shown in Fig. 10. Since stress and strain rate are proportional in fluids in general [43,44], changing the strain rate is expected to produce a sensible change in stiffness of CNT forests in solvents if the solvent is carrying a significant part of the stress (e.g., as a lubricant). Stiffness increases by 30% in the case of dry CNT forest for strain rates of 0.1–1 s^{-1}. This could be related to the viscoelastic nature of dry CNT forests, which has been shown in previous reports [9,45,46]. However, changing the strain rate by two orders of magnitude produced no significant change in stiffness of wet CNT forest. This shows that the effect of viscous drag is not a principal contributor to the reduction in the stiffness of soaked CNT forest.

The results presented here agree qualitatively with previously reported effects of fluids on the mechanical properties of buckypaper or porous CNT mats. Whitten et al. [47] studied the effects of fluids on the elastic modulus of buckypaper using tensile testing of strips of buckypaper. The testing was performed on dry samples as well as samples soaked in water and the ionic liquid 1-butyl-3-methyl-imidazolium tetrafluoroborate. They measured lower modulus in the presence of fluids. As the interaction between CNTs in buckypaper have been reported to be dominant by vdW forces [48], the effect of the solvent on the elastic modulus of the buckypaper seems to be consistent with the effect of vdW forces on the stiffness of CNT forests revealed in this work.

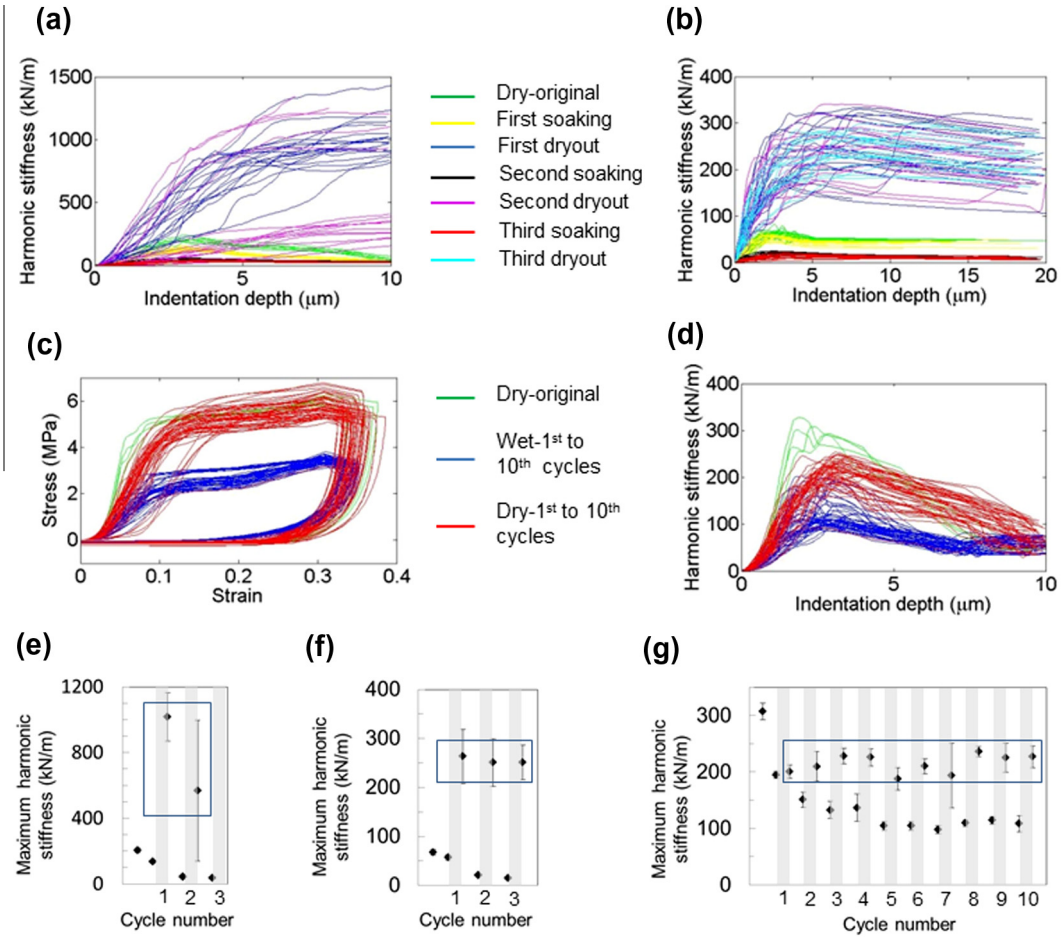

Fig. 9 – Wet–dry cycling of CNT forests. Harmonic stiffness of (a) short and (b) tall CNT forest for three wet–dry cycles with acetonitrile. (c) Stress–strain and (d) harmonic stiffness of a short CNT forest for ten wet–dry cycles with IPA. (e–g) Maximum harmonic stiffness for wet–dry cycling tests shown in a, b, and d. Each dark strip shows a cycle with the left and right points on the strips showing wet and dry states respectively. The far left point represents the original state. The rectangles enclosing the dry-out data points are shown for clarification. (A colour version of this figure can be viewed online.)

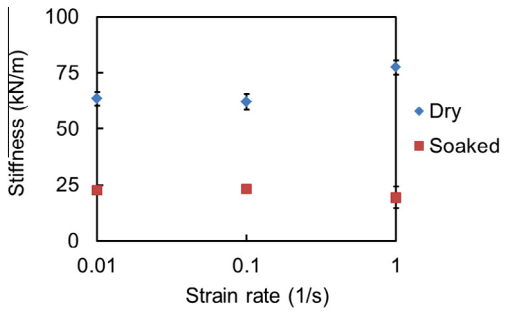

Fig. 10 – Effect of strain rate on the stiffness of a dry and a wet CNT forest. (A colour version of this figure can be viewed online.)

5. Summary

Effective stiffness and the deformation mechanism of CNT forests were evaluated in dry and solvent-soaked conditions by micro-indentation using a 100 μm diameter flat punch. We found that stiffness decreases when solvents are used as medium and that the reduction in stiffness is higher for a CNT forest with a higher original stiffness. In addition, soaking changed the deformation mechanism in compression tests. While dry CNT forests experienced local buckling concentrated at the bottom of the CNT forest, local buckles along the entire height and global buckling of the entire length of CNTs occurred in soaked CNT forests. MD simulations were also performed to quantify the vdW interaction forces between individual CNT contact points. The combination of our experimental and numerical studies provides evidence that the change in vdW forces at CNT–CNT contacts by soaking CNT forests is the major reason for the change in stiffness and deformation mechanism. Nanoindentation tests as a function of strain rate showed that viscous drag did not cause significant effects. The repeatability of the stiffness change with soaking was examined. Stiffness decreased more significantly in the cycles following the first cycle and reached a plateau value. The results suggest that soaking CNT forests in solvents could be useful for applications such as interface materials [49,50] where lower stiffness of CNT forests and higher contact area with adjacent surfaces are needed and

any application that demands reversibility and repeatability of deformation.

Acknowledgements

The authors thank Denzell Bolling, visiting undergraduate student from Howard University, for his assistance with experiments. B.A.C. is grateful for support from the U.S. Air Force Summer Faculty Fellowship Program. This work was partially supported by DARPA and the Space and Naval Warfare (SPAWAR) Systems Center, Pacific under Contract No. N66001-09-C-2013. The views expressed are those of the authors and do not reflect the official policy or position of the Department of Defense or the U.S. Government.

REFERENCES

[1] McCarter CM, Richards RF, Mesarovic SD, Richards CD, Bahr DF, McClain D, et al. Mechanical compliance of photolithographically defined vertically aligned carbon nanotube turf. J Mater Sci 2006;41(23):7872–8.
[2] Qiu A, Bahr DF, Zbib AA, Bellou A, Mesarovic SD, McClain D, et al. Local and non-local behavior and coordinated buckling of CNT turfs. Carbon 2011;49(4):1430–8.
[3] Malik H, Stephenson KJ, Bahr DF, Field DP. Quantitative characterization of carbon nanotube turf topology by SEM analysis. J Mater Sci 2011;46(9):3119–26.
[4] Raney JR, Misra A, Daraio C. Tailoring the microstructure and mechanical properties of arrays of aligned multiwall carbon nanotubes by utilizing different hydrogen concentrations during synthesis. Carbon 2011;49:3631–8.
[5] Mesarovic SD, McCarter CM, Bahr DF, Radhakrishnan H, Richards RF, Richards CD, et al. Mechanical behavior of a carbon nanotube turf. Scripta Mater 2007;56(2):157–60.
[6] Qi HJ, Teo KBK, Lau KKS, Boyce MC, Milne WI, Robertson J, et al. Determination of mechanical properties of carbon nanotubes and vertically aligned carbon nanotube forests using nanoindentation. J Mech Phys Solids 2003;51(11–12):2213–37.
[7] Cao AY, Dickrell PL, Sawyer WG, Ghasemi-Nejhad MN, Ajayan PM. Super-compressible foamlike carbon nanotube films. Science 2005;310(5752):1307–10.
[8] Cao C, Reiner A, Chung C, Chang SH, Kao I, Kukta RV, et al. Buckling initiation and displacement dependence in compression of vertically aligned carbon nanotube arrays. Carbon 2011;49:3190–9.
[9] Hutchens SB, Hall LJ, Greer JR. In situ mechanical testing reveals periodic buckle nucleation and propagation in carbon nanotube bundles. Adv Funct Mater 2010;20(14):2338–46.
[10] Maschmann MR, Ehlert GJ, Park SJ, Mollenhauer D, Maruyama B, Hart AJ, et al. Visualizing strain evolution and coordinated buckling within CNT arrays by in situ digital image correlation. Adv Funct Mater 2012;22(22):4625.
[11] Maschmann MR, Zhang Q, Wheeler R, Du F, Dai L, Baur J. In situ SEM observation of column-like and foam-like CNT array nanoindentation. ACS Appl Mater Interfaces 2011;3:648–53.
[12] Maschmann MR, Zhang QH, Du F, Dai LM, Baur J. Length dependent foam-like mechanical response of axially indented vertically oriented carbon nanotube arrays. Carbon 2011;49(2):386–97.
[13] Barber AH, Andrews R, Schadler LS, Wagner HD. On the tensile strength distribution of multiwalled carbon nanotubes. Appl Phys Lett 2005;87(20):203106.
[14] Abadi Parisa Pour Shahid Saeed, Hutchens SB, Greer JR, Cola BA, Graham S. Effects of Morphology on the micro-compression response of carbon nanotube forests. Nanoscale 2012;4(11):8.
[15] Gao Y, Kodama T, Won Y, Dogbe S, Pan L, Goodson KE. Impact of nanotube density and alignment on the elastic modulus near the top and base surfaces of aligned multi-walled carbon nanotube films. Carbon 2012;50(10):3789–98.
[16] Nguyen JJ, Bougher TL, Abadi Parisa Pour Shahid Saeed, Sharma A, Graham S, Cola BA. Post-growth microwave treatment to align carbon nanotubes. J Micro Nano-Manuf 2013;1:014501–7.
[17] Lu Y, Joseph J, Maschmann M, Dai L, Baur J. Rate-dependent, large-displacement deformation of vertically aligned carbon nanotube arrays. In: Challenges in mechanics of time-dependent materials and processes in conventional and multifunctional materials. New York: Springer; 2013. p. 101–7.
[18] Pathak S, Mohan N, Abadi PPSS, Graham S, Cola BA, Greer JR. Compressive response of vertically aligned carbon nanotube films gleaned from in situ flat-punch indentations. J Mater Res 2013;28(7):984–97.
[19] Pathak S, Lim EJ, Abadi Parisa Pour Shahid Saeed, Graham S, Cola BA, Greer JR. Higher recovery and better energy dissipation at faster strain rates in carbon nanotube bundles: an in-situ study. ACS Nano 2012;6(3):2189–97.
[20] Maschmann MR, Ehlert GJ, Park SJ, Mollenhauer D, Maruyama B, Hart AJ, et al. Visualizing strain evolution and coordinated buckling within CNT arrays by in situ digital image correlation. Adv Funct Mater 2012;22(22):4686–95.
[21] Radhakrishnan H, Mesarovic SD, Qiu A, Bahr DF. Phenomenological constitutive model for a CNT turf. Int J Solids Struct 2013;50(14–15):2224–30.
[22] Abadi Parisa Pour Shahid Saeed, Hutchens SB, Greer JR, Cola BA, Graham S. Buckling-driven delamination of carbon nanotube forests. Appl Phys Lett 2013;102(22):223103.
[23] Hiemenz PC, Rajagopalan R. Principles of colloid and surface chemistry. 3rd ed. New York: Marcel Dekker; 1997.
[24] Garcia EJ, Hart AJ, Wardle BL, Slocum AH. Fabrication of composite microstructures by capillarity-driven wetting of aligned carbon nanotubes with polymers. Nanotechnology 2007;18(16).
[25] Tawfick S, De Volder M, Hart AJ. Structurally programmed capillary folding of carbon nanotube assemblies. Langmuir 2011;27(10):6389–94.
[26] Zhao ZZ, Tawfick SH, Park SJ, De Volder M, Hart AJ, Lu W. Bending of nanoscale filament assemblies by elastocapillary densification. Phys Rev E 2010;82(4):11–2.
[27] Liu Z, Bajwa N, Ci L, Lee SH, Kar S, Ajayan PM, et al. Densification of carbon nanotube bundles for interconnect application. In: Proceedings of the IEEE 2007 international interconnect technology conference, 2007. p. 201–203.
[28] De Volder MFL, Park SJ, Tawfick SH, Vidaud DO, Hart AJ. Fabrication and electrical integration of robust carbon nanotube micropillars by self-directed elastocapillary densification. J Micromech Microeng 2011;21(4):045033.
[29] Qiu A, Bahr DF. The role of density in the mechanical response of CNT turfs. Carbon 2013;55:335–42.
[30] Pushparaj V, Mahadevan L, Sreekala S, Ci L, Nalamasu R, Ajayan PM. Deformation and capillary self-repair of carbon nanotube brushes. Carbon 2012;50(15):5618–20.
[31] Tawfick S, Zhao Z, Maschmann M, Brieland-Shoultz A, De Volder M, Baur JW, et al. Mechanics of capillary forming of aligned carbon nanotube assemblies. Langmuir 2013;29(17):5190–8.
[32] Taphouse JH, Bougher TL, Singh V, Abadi PPSS, Graham S, Cola BA. Carbon nanotube thermal interfaces enhanced with

sprayed on nanoscale polymer coatings. Nanotechnology 2013;24(10):105401.
[33] Taphouse JH, Smith OL, Marder SR, Cola BA. A pyrenylpropyl phosphonic acid surface modifier for mitigating the thermal resistance of carbon nanotube contacts. Adv Funct Mater 2013. http://dx.doi.org/10.1002/adfm.201301714.
[34] Hess B, Kutzner C, van der Spoel D, Lindahl E. GROMACS 4: algorithms for highly efficient, load-balanced, and scalable molecular simulation. J Chem Theory Comput 2008;4(3):435–47.
[35] Oliver WC, Pharr GM. An improved technique for determining hardness and elastic modulus using load and displacement sensing indentation experiments. J Mater Res 1992;7(06):1564–83.
[36] Bedewy M, Meshot ER, Guo HC, Verploegen EA, Lu W, Hart AJ. Collective mechanism for the evolution and self-termination of vertically aligned carbon nanotube growth. J Phys Chem C 2009;113(48):20576–82.
[37] Van Oss CJ, Chaudhury MK, Good RJ. Interfacial Lifshitz-van der Waals and polar interactions in macroscopic systems. Chem Rev 1988;88(6):927–41.
[38] Xu D, Ravi-Chandar K, Liechti KM. On scale dependence in friction: transition from intimate to monolayer-lubricated contact. J Colloid Interface Sci 2008;318(2):507–19.
[39] Rajter RF, Podgornik R, Parsegian VA, French RH, Ching WY. Van der Waals–London dispersion interactions for optically anisotropic cylinders: metallic and semiconducting single-wall carbon nanotubes. Phys Rev B 2007;76(4).
[40] Takenaga M, Jo S, Graupe M, Lee TR. Effective van der Waals surface energy of self-assembled monolayer films having systematically varying degrees of molecular fluorination. J Colloid Interface Sci 2008;320(1):264–7.
[41] Birdi KS. Handbook of surface and colloidal chemistry. 3rd ed. NY, USA: CRC Press; 2008.
[42] Rajter RF, French RH, Ching WY, Carter WC, Chiang YM. Calculating van der Waals–London dispersion spectra and Hamaker coefficients of carbon nanotubes in water from ab initio optical properties. J Appl Phys 2007;101(5).
[43] Kay JM, Nedderman RM. Fluid mechanics and transfer processes. Cambridge Cambridgeshire, New York, N.Y.: Cambridge University Press; 1985.
[44] Chhabra RP, Richardson JF. Non-newtonian flow in the process industries: fundamentals and engineering applications. Oxford; Boston, MA: Butterworth–Heinemann; 1999.
[45] Pathak S, Cambaz ZG, Kalidindi SR, Swadener JG, Gogotsi Y. Viscoelasticity and high buckling stress of dense carbon nanotube brushes. Carbon 2009;47(8):1969–76.
[46] Zhang Q, Lu Y, Du F, Dai L, Baur J, Foster D. Viscoelastic creep of vertically aligned carbon nanotubes. J Phys D: Appl Phys 2010;43:315401.
[47] Whitten PG, Spinks GM, Wallace GG. Mechanical properties of carbon nanotube paper in ionic liquid and aqueous electrolytes. Carbon 2005;43(9):1891–6.
[48] Coleman JN, Blau WJ, Dalton AB, Munoz E, Collins S, Kim BG, et al. Improving the mechanical properties of single-walled carbon nanotube sheets by intercalation of polymeric adhesives. Appl Phys Lett 2003;82(11):1682–4.
[49] Cola BA, Xu J, Fisher TS. Contact mechanics and thermal conductance of carbon nanotube array interfaces. Int J Heat Mass Transfer 2009;52(15–16):3490–503.
[50] Abadi Parisa Pour Shahid Saeed, Chung DDL. Numerical modeling of the performance of thermal interface materials in the form of paste-coated sheets. J Electron Mater 2011;40(7):1490–500.